

Terahertz plasmonic high pass filter

Dongmin Wu, Nicholas Fang, Cheng Sun, Xiang Zhang, Willie J. Padilla, Dimitri N. Basov, David R. Smith, and Sheldon Schultz

Citation: [Applied Physics Letters](#) **83**, 201 (2003); doi: 10.1063/1.1591083

View online: <http://dx.doi.org/10.1063/1.1591083>

View Table of Contents: <http://scitation.aip.org/content/aip/journal/apl/83/1?ver=pdfcov>

Published by the [AIP Publishing](#)

Articles you may be interested in

[Broadband ultra-low-loss mesh filters on flexible cyclic olefin copolymer films for terahertz applications](#)
Appl. Phys. Lett. **102**, 111114 (2013); 10.1063/1.4798522

[Metamaterial high pass filter based on periodic wire arrays of multiwalled carbon nanotubes](#)
Appl. Phys. Lett. **97**, 163102 (2010); 10.1063/1.3491840

[A tunable universal terahertz filter using artificial dielectrics based on parallel-plate waveguides](#)
Appl. Phys. Lett. **97**, 131106 (2010); 10.1063/1.3495994

[Optically controllable transfective spatial filter with high- and low-pass or notch- and band-pass functions based on a dye-doped cholesteric liquid crystal film](#)
Appl. Phys. Lett. **92**, 011121 (2008); 10.1063/1.2832367

Terahertz frequency bandpass filters

J. Appl. Phys. **102**, 023102 (2007); 10.1063/1.2756072



Terahertz plasmonic high pass filter

Dongmin Wu, Nicholas Fang, Cheng Sun, and Xiang Zhang^{a)}

Department of Mechanical and Aerospace Engineering, University of California at Los Angeles, 420 Westwood Plaza, Los Angeles, California 90095

Willie J. Padilla, Dimitri N. Basov, David R. Smith, and Sheldon Schultz

Department of Physics, University of California at San Diego, 9500 Gilman Drive, La Jolla, California 92093

(Received 13 January 2003; accepted 15 May 2003)

Metamaterials, which contain engineered subwavelength microstructures, can be designed to have positive or negative ϵ and μ at desired frequencies. In this letter, we demonstrate a metamaterial which has a “plasmonic” response to electromagnetic waves in the terahertz (THz) range. The sharp change of reflection and transmission at this plasma frequency makes the structure a high pass filter. The reflection response is characterized by Fourier transform infrared spectroscopy, and a plasma frequency at 0.7 THz is observed, which agrees with the theoretical calculation. The metamaterial is a two-dimensional cubic lattice consisting of thin metal wires, having wire diameter of 30 μm , lattice constant of 120 μm , and wire length of 1 mm. The microstereolithography technique is employed to fabricate the high-aspect-ratio lattice. © 2003 American Institute of Physics.
[DOI: 10.1063/1.1591083]

Electromagnetic metamaterials, formed by artificial subwavelength components, are developed to provide designers with materials with properties that are not available in naturally existing materials. Many exciting applications can be expected from these microstructured materials. Artificial magnetic material,¹ for example, can be realized by arrays of metallic, nonmagnetic split-ring or “Swiss roll” resonant structures. Left-handed,^{2,3} or negative refraction material is another exciting example of metamaterials, which is proposed to make a so-called “superlens” that can focus the image beyond the diffraction limit. Recently, a few experiments reported the existence of a GHz frequency plasmonic behavior in thin metal wire structures, with the effective plasma frequency much lower than in bulk metals.^{4,5} Realization of the plasmonic structure in THz ranges may lead to applications such as a high pass filter in the THz imaging system⁶ to reject thermal radiation signals.^{7,8} In this letter, we demonstrate a THz plasmonic high pass filter consisting of high-aspect-ratio micron-sized wire arrays fabricated by microstereo-lithography (μSL).

For bulk metal materials, the free electron gas theory predicts the response to electromagnetic (EM) wave. The frequency dependent permittivity of metal is described by the Drude model as

$$\epsilon(\omega) = 1 - \frac{\omega_p^2}{\omega^2}, \quad (1)$$

where ω_p is the plasma frequency, which is related to the electron density n , electron mass m_e , and charge e as

$$\omega_p^2 = \frac{ne^2}{\epsilon_0 m_e}. \quad (2)$$

For most metals, the free electron density is at the order of 10^{22} cm^{-3} , and the plasma frequency ω_p is in the range of visible to ultraviolet (UV) wavelength.

Many engineering applications require lowering the plasma frequency from optical to infrared, THz, and microwave range. One way to lower the plasma frequency is by adjusting the electron density of the materials through “diluting” metal, by engineering the subwavelength metallic structures. According to Pendry *et al.*,⁴ for a two-dimensional (2D) subwavelength lattice of thin-wire metal structures subjected to the EM irradiation with electric field parallel to the wires, the collective EM response of the microstructured material is characterized by a lower effective plasma frequency

$$\omega_p^2 = \frac{2\pi c_0^2}{a^2 \ln(a/r)}, \quad (3)$$

where c_0 is the velocity of light in vacuum, a is the lattice constant of the 2D wire array, r is the radius of the cylinder wire. The plasma frequency is not only reduced by diluting the effective electron density measured in the order of wavelength, but also by increasing the effective electron mass due to the induced current on the wire and, subsequently, the magnetic field around the wire. The effective plasma frequency strongly depends on the lattice constant and the wire radius. This finding provides an interesting method to tune the plasma frequency by adjusting the geometric parameters of metamaterials. For EM waves with frequency lower than ω_p , the effective permittivity of the thin metal structure will be negative, according to Eq. (1), and no propagating mode exists inside the structure. Above the plasma frequency, the effective permittivity is positive and the EM wave is allowed to propagate through the structure. The reflection coefficient at normal incidence of such a metamaterial can be calculated from the Fresnel equation

^{a)}Author to whom correspondence should be addressed; electronic mail: xiang@seas.ucla.edu

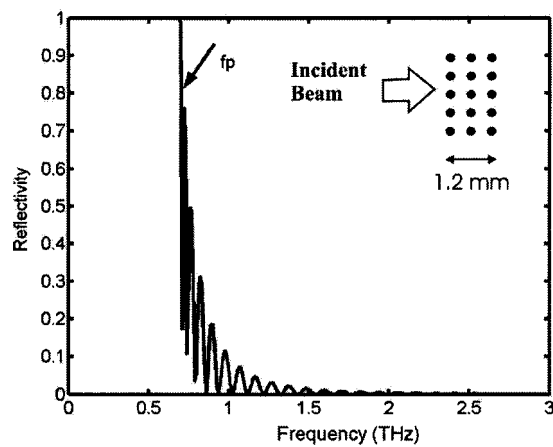


FIG. 1. The reflectivity of the thin wire metal structure calculated from Eq. (4). The electric field of normal incident beam is parallel to the wire. The small peaks come from the multiple reflections from the film interface (film thickness is 1.2 mm).

$$R = \left| \frac{\left(\frac{k_0/\varepsilon_0 - k_1/\varepsilon_1}{k_0/\varepsilon_0 + k_1/\varepsilon_1} \right) [1 - \exp(-2ik_1d)]}{1 - \left(\frac{k_0/\varepsilon_0 - k_1/\varepsilon_1}{k_0/\varepsilon_0 + k_1/\varepsilon_1} \right)^2 \exp(-2ik_1d)} \right|^2, \quad (4)$$

where k_0 , ε_0 and k_1 , ε_1 are the wave vector and permittivity in air and the metamaterial, respectively, d is the thickness of the metamaterial. The value of ε_1 is frequency dependent and can be calculated from Eqs. (1) and (3). For example, 2D cubic lattice with $a=120 \mu\text{m}$, $r=15 \mu\text{m}$, has an effective plasma frequency $f_p = \omega_p/2\pi$ calculated from Eq. (3) of about 0.7 THz. Substituting Eqs. (1) and (3) into Eq. (4) and taking d as 1.2 mm according to our sample size, the frequency dependent reflection coefficient is calculated as shown in Fig. 1. A rapid drop of the reflection at the plasma frequency f_p is expected from the calculation. The small peaks in the plot result from multiple reflections at the interfaces. The plasmonic behavior of our structure strongly depends on the polarization of the incident beam. With the electric field perpendicular to the wire, simulations show that the transmission band of the 2D metal cubic lattice approaches zero frequency.⁹

To apply this effective media theory the length of the wire must be much longer than the wavelength,⁴ which means the aspect ratio of the wire is very high. It is difficult to use traditional silicon micromachining techniques to fabricate such structures. We employed a μSL system^{10,11} to synthesize these high-aspect-ratio cylinders. Figure 2 shows the working principle of the μSL system. The beam shaping element delivers the mask pattern to the projection lens, which focuses the UV light on the surface of the resin. The liquid resin contains monomer and photoinitiator and thus can be photocross-linked by the UV exposure. Under the exposure, a thin layer of solid polymer structure is formed by the computer generated mask pattern according to the sliced cross section of the digital three-dimensional (3D) model. By stacking the layers sequentially in the course of lowering the elevator, one can fabricate a solid polymer copy of the digital 3D model out of the liquid resin. After the μSL fabrication, the polymerized structure is immersed in acetone to remove the uncured resin and postcuring in an UV oven is executed

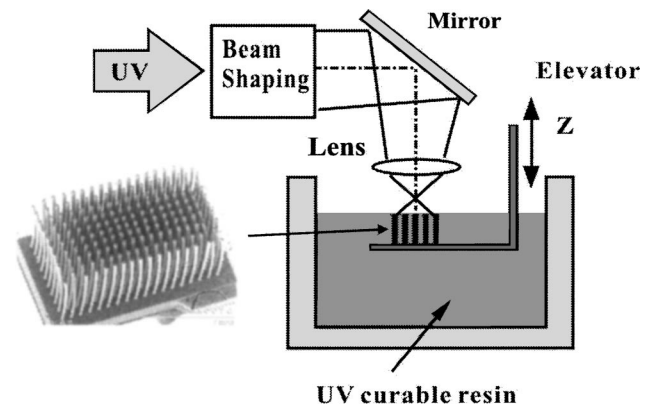


FIG. 2. The 3D structure is fabricated with a layer-by-layer photopolymerization of the UV curable liquid resin. The cross-section pattern of digital 3D model is delivered by the beam shaping system and focused by the projection lens on the UV resin surface. The elevator will move down after one layer is exposed, allowing the new layer to be formed on the surface.

to enhance the mechanical strength of the wires.¹² After post-curing, the structure is released from the acetone. Certain deformation of the wires at the outer layer of the 2D lattice is due to the capillary force during release [see the inset scanning electron microscope (SEM) picture in Fig. 2]. These deformations are justified as lattice defects, and may cause noises in measured EM wave response.

Figure 3 shows the SEM image of the 2D cubic lattice of thin wires. These wires have a lattice constant of $120 \mu\text{m}$, diameter of $30 \mu\text{m}$, and length of 1 mm, corresponding to an aspect ratio larger than 30. The whole structure has dimensions of $2.1 \times 1.2 \times 1.0 \text{ mm}$. After μSL fabrication, a thin film of gold is sputtered uniformly on the polymer structures to ensure adequate conductivity. To reduce the shadowing effects, the sputtering deposition was done in four steps. In each step, the sample was tilted 20° and rotated in 0° , 90° , 180° and 270° , respectively, to ensure the good homogeneity of Au coating along the cylinders. Copper electroplating is performed to check the continuity of the Au film on the polymer structures, although the final structure for Fourier transform infrared (FTIR) measurement does not have electroplated copper. The gold thickness is about $0.3 \mu\text{m}$, larger than the skin depth of the THz radiation in Au (80 nm at 1 THz). Therefore, in this frequency range we can treat the

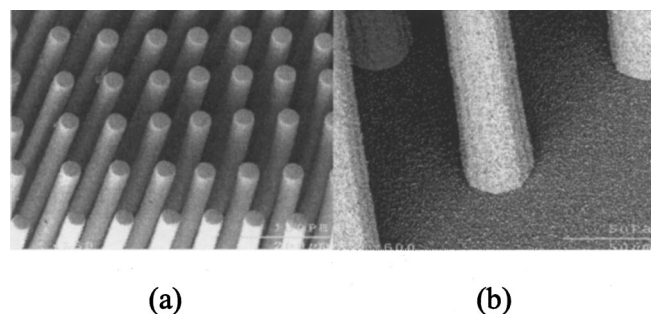


FIG. 3. Environmental SEM picture of the 2D cubic lattice fabricated by advanced μSL . Lattice constant $a=120 \mu\text{m}$, wire radius $r=15 \mu\text{m}$, wire length $l=1 \text{ mm}$; the dimension of whole structure is $2.1 \times 1.2 \times 1 \text{ mm}$. (a) The original polymer structure before gold coating, (b) after gold coating and copper electroplating. (b) Indicates the continuity of the gold coating along the polymer wires. No shadowing effect is observed.

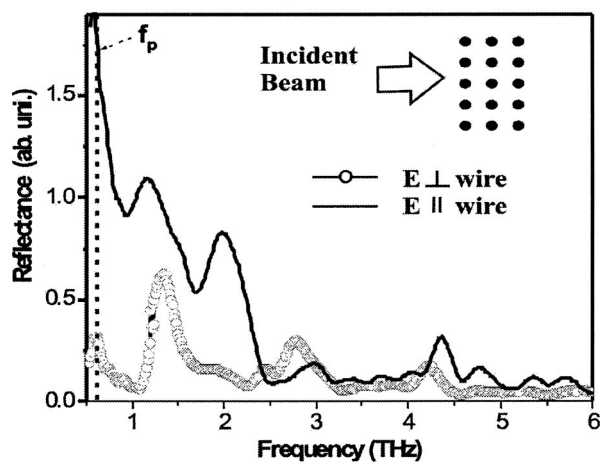


FIG. 4. Reflection signal from FTIR measurement. The solid line corresponding to the reflection signal for E filed parallel to the wire, and a rapid drop of the signal is observed above the plasma frequency (~ 0.7 THz). As for perpendicular polarization (threaded circles), the reflectivity is low at 0.7 – 1.2 THz, indicating a transparent window.

whole wire as metallic without considering the contribution of embedded polymer.

The reflectance measurements were performed using a FTIR spectroscopy in the range of 0.6 – 6 THz with a near normal incident beam at room temperature. The polarized light was aligned either parallel (E field parallel to the wire) or perpendicular to the wires. In our FTIR experiment, we used a collimated source (minimum diameter 5 mm) to illuminate a freestanding plasmonic filter. The sample size is 1 mm, corresponding to 2 – 3 wavelengths in the frequency range of interest. From diffraction theory, we estimated that the intensity within 10° divergence is $\sim 60\%$ of the total reflected intensity. Thus the optical theorem remains a good approximation, and the scattering effects will not smear the plasmonic edge in the measured reflection signal. Certainly, a transmission measurement will provide a direct indication of the high pass filtering performance of the plasmonic devices, as demonstrated in Ref. 13 where a focused beam is used. This is not yet available in our setup, and a waveguide characterization system will be developed for future work. Figure 4 shows the reflectance of the THz structure in both orientations. For the perpendicular polarization, the reflectance is low within the frequency range measured, (apart from several peaks), indicating a transmission band that agrees with theory. For the parallel orientation the response is dramatically different. The reflectance drops rapidly at 0.7 THz to small values comparable to the value in the perpendicular

orientation. This subwavelength structure forms a THz high pass filter. The observed plasma frequency of 0.7 THz is in good agreement with the theoretical value calculated from Eq. (3). We also observed some small peaks above the plasma frequency in both parallel and perpendicular polarization. These small peaks cannot be explained by the multiple reflections from the film interface as shown in Fig. 1, because the peak positions and spacing do not match each other. These small peaks may be due to the effect of lattice deformation from the outer layer of the structure, as mentioned previously.

In conclusion, we have demonstrated a THz plasmonic high pass filter. The subwavelength 2D cubic lattice of metallic wire arrays has a plasma frequency at 0.7 THz. The reflection signal is measured using FTIR for different polarizations. The measured plasma frequency agrees well with theory. This plasmonic property of the microstructured material can be used as high pass filters at desired frequency, by designing the geometrical parameters of the structure. These 2D metal wire arrays can also be used as a high efficiency polarization filter in THz optics by virtue of their anisotropic response to the EM wave.

This work is supported by the Department of Defense Multidisciplinary University Research Initiative (MURI) under Grant No. N00014-01-1-0803, the Office of Naval Research (ONR) Young Investigator Award under Grant No. N00014-02-1-0224, and the National Science Foundation (NSF) CAREER Award under Grant No. DMI-0196395.

¹M. C. K. Wiltshire, J. B. Pendry, I. R. Young, D. J. Larkman, D. J. Gilderdale, and J. V. Hajnal, *Science* **291**, 849 (2001).

²J. B. Pendry, *Phys. Rev. Lett.* **85**, 3966 (2000).

³R. A. Shelby, D. R. Smith, and S. Schultz, *Science* **292**, 77 (2001).

⁴J. B. Pendry, A. J. Holden, D. J. Robbins, and W. J. Stewart, *J. Phys.: Condens. Matter* **10**, 4785 (1998).

⁵P. Gay-Balmaz, C. Maccio, and O. J. F. Martin, *Appl. Phys. Lett.* **81**, 2896 (2002).

⁶V. M. Lubecke, K. Mizuno, and G. M. Rebeiz, *IEEE Trans. Microwave Theory Tech.* **46**, 1821 (1998).

⁷M. E. MacDonald, A. Alexanian, R. A. York, Z. Popovic, and E. N. Grossman, *IEEE Trans. Microwave Theory Tech.* **48**, 712 (2000).

⁸G. Gruner, *Millimeter and Submillimeter Wave Spectroscopy of Solids* (Springer, Berlin, 1998).

⁹L. M. Li, Z. Q. Zhang, and X. D. Zhang, *Phys. Rev. B* **58**, 15589 (1998).

¹⁰D. Wu, N. Fang, C. Sun, and X. Zhang, *Appl. Phys. Lett.* **81**, 3963 (2002).

¹¹X. Zhang, X. N. Jiang, and C. Sun, *Sens. Actuators A* **77**, 149 (1999).

¹²E. Manias, J. Chen, N. Fang, and X. Zhang, *Appl. Phys. Lett.* **79**, 1700 (2001).

¹³N. Atsarakis, M. Bender, L. Singleton, G. Kiriakidis, and C. M. Soukoulis, *Microsystem Technologies*, **8**, 74 (2002).